



ELSEVIER

Contents lists available at ScienceDirect

ISA Transactions

journal homepage: www.elsevier.com/locate/isatrans

Research Article

Fractional active disturbance rejection control

Dazi Li^{a,*}, Pan Ding^a, Zhiqiang Gao^b^a Institute of Automation, Beijing University of Chemical Technology, Beijing 100029, PR China^b Center for Advanced Control Technologies, Cleveland State University, Cleveland, OH 44115, USA

ARTICLE INFO

Article history:

Received 3 June 2015

Received in revised form

5 January 2016

Accepted 29 January 2016

Available online 28 February 2016

Keywords:

Fractional active disturbance rejection control (FADRC)

Fractional extended state observer (FESO)

Fractional proportional-derivative controller

Linear fractional order system (FOS)

ABSTRACT

A fractional active disturbance rejection control (FADRC) scheme is proposed to improve the performance of commensurate linear fractional order systems (FOS) and the robust analysis shows that the controller is also applicable to incommensurate linear FOS control. In FADRC, the traditional extended states observer (ESO) is generalized to a fractional order extended states observer (FESO) by using the fractional calculus, and the tracking differentiator plus nonlinear state error feedback are replaced by a fractional proportional-derivative controller. To simplify controller tuning, the linear bandwidth-parameterization method has been adopted. The impacts of the observer bandwidth ω_o and controller bandwidth ω_c on system performance are then analyzed. Finally, the FADRC stability and frequency-domain characteristics for linear single-input single-output FOS are analyzed. Simulation results by FADRC and ADRC on typical FOS are compared to demonstrate the superiority and effectiveness of the proposed scheme.

© 2016 ISA. Published by Elsevier Ltd. All rights reserved.

1. Introduction

Fractional calculus is the generalization of ordinary integer order calculus. Systems described by fractional order calculus are known as fractional order systems (FOS). Fractional calculus provides a preferable method to describe complicated natural objects and dynamical processes such as electrical noises, chaotic system, and organic dielectric materials [1–6]. As a consequence, scientists show more and more interests in identification of FOS [7,8]. Commensurate linear FOS is a special kind of FOS, with a simple model and proportional orders [9,10].

Controllers with fractional order operator are naturally suitable for the FOS [11,12]. There are mainly four kinds of fractional order controllers, which are CRONE (Contrôle Robuste d'Order Non Entier) controller, TID (Tilt Integral Derivative) controller, fractional order PID controller, and fractional order lead-lag compensator [13–19]. Considering the industrial universal controller design requirements, such as compact structure, repeatability, model independence, easy parameter turning and strong robustness, active disturbance rejection control (ADRC) provides an alternative paradigm for FOS control [20–22]. The central objective of ADRC is to treat the internal and external uncertainties as the total disturbance and to reject them actively. Compact frame, effortless turning and sufficiently good performance make ADRC

popular in the world of industrial control [23–25]. ADRC was firstly used to control FOS in [26], where fractional order is regarded as a part of the total disturbances, and an extended state observer (ESO) is used to estimate and reject it. Because the known or available model information is neglected and under-used, it would require higher observer bandwidth for accurate state estimation. In this paper, a distinct fractional active disturbance rejection control (FADRC) is proposed as a generalized and enhanced ADRC solution for the FOS. ESO is redesigned as a fractional one according to the highest fractional order of FOS. The modified fractional extended states observer (FESO) not only accurately estimates the total disturbance but also the fractional order dynamic states, leading to a reduced observer bandwidth. In addition, a fractional order PD controller is used to replace the tracking differentiator and the nonlinear state error feedback. Although FADRC is designed for commensurate linear FOS originally, the robustness analyses demonstrate that FADRC is also appropriate for incommensurate linear FOS. Simulation results show that FADRC has more inherent superiority and potential for FOS control.

Due to the difficulty brought by the nonlinearity and uncertainty, theoretical studies of ADRC are still lagging behind its industrial applications. Recent research focuses on time domain convergence, frequency response and describing function in analyzing nonlinearity [27–29]. Stability analysis has been substantially studied for FOS in [30]. An extended root locus method by Patil [31] provides a simple way to construct root locus of general FOS and is employed for FADRC analysis and design.

* Correspondence to: School of Information Science and Technology, Beijing University of Chemical Technology, P.O. box No. 81, Beijing 100029, PR China. Tel.: +86 10 64434930; fax: +86 10 64437805.

E-mail address: lidz@mail.buct.edu.cn (D. Li).

The FOS is translated into its integer order counterpart and then analysis method of general integer system can be directly adopted.

The rest of this paper is organized as follows. In Section 2, an introduction of commensurate linear FOS and fractional order state observer with full-dimensionality are presented. In Section 3, the framework of FESO and FADRC and the corresponding algorithm are introduced. Section 4 presents the stability and frequency-domain characteristics of FADRC. Simulation results of FADRC and ADRC are then compared in Section 5. Finally, conclusions are given in Section 6.

2. Fractional order systems and fractional order state observer with full-dimensionality

The conventional integer order single input single output (SISO) transfer function can be extended to the case of the FOS. There exist various alternative definitions of the fractional derivative, and the Grünwald–Letnikov (GL), Riemann–Liouville (RL) and Caputo definitions are mainly used. In all of the three definitions, the fractional operator acts as a non-local operator, and that is to say fractional derivatives have a memory of the past values.

It is difficult to directly implement the fractional order operator in time-domain for the complicated FOS by using the standard definitions. To solve this problem, the normative integer-order operators are applied to approximate fractional order operators. A lot of works and researches have been done in this area. Piché gives the discrete-time approximations of fractional order operators based on numerical quadrature [32]. Freeborn proposed a method to reduce the second-order approximation ripple error of the fractional order differential operator [33]. The approximation listed in [34] is adopted in this paper, which is based on network theory approximations, and the approximation can give desired accuracy over any frequency band.

2.1. Transfer function representation

A SISO linear FOS can be described as [35]:

$$y(t) + \sum_{i=0}^n a_{it_0} D_t^{\phi_i} y(t) = \sum_{j=0}^m b_{jt_0} D_t^{\varphi_j} u(t), \quad (1)$$

where $u(t)$ is the input, $y(t)$ is the output, $\phi_i (1 \leq i \leq n)$ and $\varphi_j (0 \leq j \leq m)$ are real positive numbers, and $\phi_1 < \phi_2 \dots < \phi_n, \varphi_1 < \varphi_2 \dots < \varphi_m (\varphi_m < \phi_n)$. Model coefficients $a_i (1 \leq i \leq n)$ and $b_j (0 \leq j \leq m)$ are constants. ${}_0 D_t^\alpha (\alpha = \varphi_i \text{ or } \alpha = \phi_j)$ is a fractional order differential operator, t_0 and t denote the upper and lower limit of the integral interval, respectively. The Caputo's fractional derivative of order α with variable t and starting point $t_0=0$ is defined as follows:

$${}_0 D_t^\alpha y(t) = \frac{1}{\Gamma(1-\gamma)} \int_0^t \frac{y^{(m+1)}(\tau)}{(t-\tau)^\gamma} d\tau, \quad (2)$$

where $\Gamma(Z)$ is Euler's gammafunction, and $\alpha = m + \gamma, m \in \mathbb{N}_+, 0 < \gamma \leq 1$. In the fractional differential Eq. (1), if the order

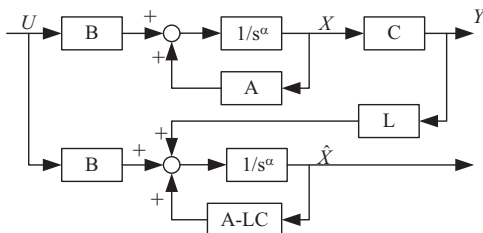


Fig. 1. Block diagram of fractional order state observer.

differentiations are integer multiples of a single based order: i.e. $\phi_i = i\alpha, \varphi_j = j\alpha$, the system will be termed as commensurate order and takes the following form:

$$y(t) + \sum_{i=0}^n a_{i0} D_t^{i\alpha} y(t) = \sum_{j=0}^m b_{j0} D_t^{j\alpha} u(t). \quad (3)$$

With zero initial conditions, the Laplace transform of Eq. (3) becomes

$$G(s) = \frac{Y(s)}{U(s)} = \frac{\sum_{j=0}^m b_j s^{j\alpha}}{1 + \sum_{i=1}^n a_i s^{i\alpha}}. \quad (4)$$

2.2. Fractional order state observer with full-dimensionality

As is well known, a commensurate FOS admits the following state-space representation:

$$\begin{cases} {}_0 D_t^\alpha x(t) = Ax(t) + Bu(t) \\ y(t) = Cx(t) \end{cases}, \quad (5)$$

where matrix A, B , and C are constants. A new fractional order state observer with full-dimensionality for the commensurate linear FOS is obtained by generalizing the classical Luenberger state observer [36], and the structure of the state observer is shown in Fig. 1. where L is the undetermined coefficient matrix, and $1/s^\alpha$ represents the fractional order integer operator. The observer error can be expressed as $E = X - \hat{X}$, where X is the actual state and \hat{X} is the estimated state.

$${}_0 D_t^\alpha E = (A - LC)E. \quad (6)$$

When the eigenvalues of matrix $(A - LC)$ stay in the stable region, Eq. (6) will be asymptotically stable (refer to Section 4 for details).

3. The structure of the fractional active disturbance rejection controller

The traditional ADRC consists of three main parts: the tracking differentiator (TD), the ESO, and the nonlinear state error feedback (NLSEF). TD is used to provide the transient process and its derivative of the input signal. ESO is used to estimate the states plus the total disturbance. After the aforementioned state variables have been obtained, NLSEF is applied to combine them and obtain the control signal. By the efforts of Gao, the bandwidth-parameterization method was proposed to linearize the ESO and PD controller without losing high precision and efficiency [37,38]. In this section, the structure of FADRC is presented. Compared with traditional ADRC, ESO is replaced by a FESO while NLSEF is replaced by a linear fractional PD controller. A second-order FADRC is shown in Fig. 2, where $v_0(t)$ and $y(t)$ represent the setpoint and output, respectively, while $u_0(t)$ denotes the output of linear fractional PD controller, $u(t)$ is the control signal, and $w(t)$ is the external disturbance. Particularly, $z_1(t), z_2(t)$ and $z_3(t)$ are the outputs of FESO, and \hat{b} is a system-dependent coefficient.

3.1. Design of fractional extended states observer

A second order linear FOS with commensurate order α is assumed as follows

$$\frac{Y(s)}{U(s)} = \frac{b}{s^{2\alpha} + a_2 s^\alpha + a_1}. \quad (7)$$

where a_2, a_1, b and $\alpha(0 < \alpha < 1)$ are constants. Its differential equation form is

$$y^{(2\alpha)} = (-a_2 y^{(\alpha)} - a_1 y) + bu = f(y^{(\alpha)}, y, t) + bu. \quad (8)$$

Particularly, let $x_1 = y, x_2 = y^{(\alpha)}$ and $x_3 = f(y^{(\alpha)}, y, t)$, among which x_1, x_2 represent the system states and x_3 is the external

state. Then, the augmented state space form of Eq. (7) can be represented as:

$$\begin{cases} x^{(\alpha)} = Ax + Bu + Eh \\ y = Cx \end{cases}, \quad (9)$$

where $x^{(\alpha)} = \begin{bmatrix} x_1^{(\alpha)} \\ x_2^{(\alpha)} \\ x_3^{(\alpha)} \end{bmatrix}, x = \begin{bmatrix} x_1 \\ x_2 \\ x_3 \end{bmatrix}, A = \begin{bmatrix} 0 & 1 & 0 \\ 0 & 0 & 1 \\ 0 & 0 & 0 \end{bmatrix}, B = \begin{bmatrix} 0 \\ b \\ 0 \end{bmatrix},$
 $C = [1 \ 0 \ 0], E = \begin{bmatrix} 0 \\ 0 \\ 1 \end{bmatrix},$ and $h = f^{(\alpha)}(\bullet)$

A linear FESO is designed to estimate the states $x_1, x_2,$ and x_3 in the following.

$$\begin{cases} z^{(\alpha)} = Az + \widehat{B}u + L(y - \hat{y}) \\ \hat{y} = Cz \end{cases}, \quad (10)$$

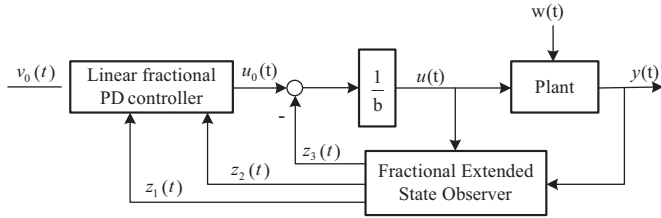


Fig. 2. Configuration of a second-order FADRC.

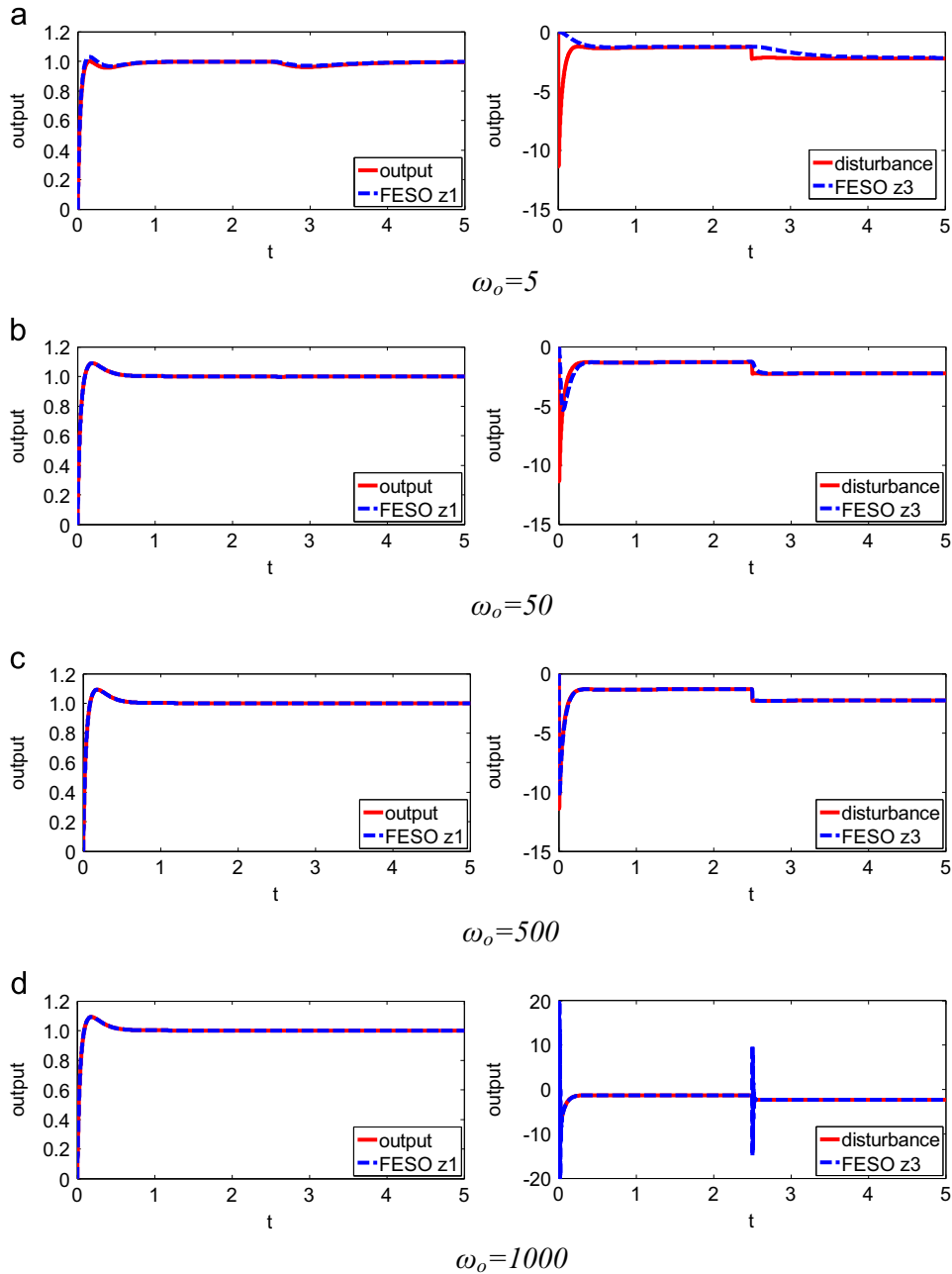


Fig. 3. Tracking responses with different ω_o . (a) $\omega_o = 5$, (b) $\omega_o = 50$, (c) $\omega_o = 500$, and (d) $\omega_o = 1000$.

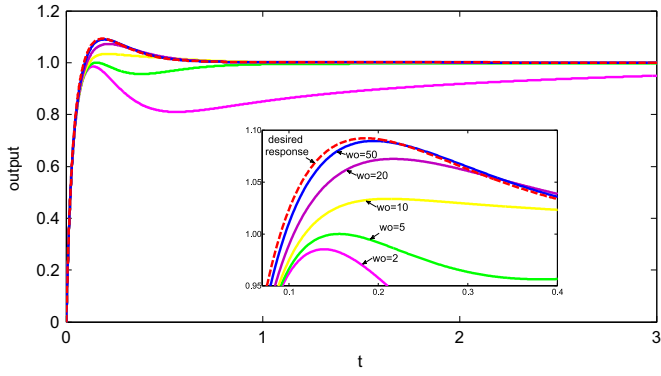


Fig. 4. Desired response and system outputs with different ω_o .

where

$$z^{(\alpha)} = [z_1^{(\alpha)} \quad z_2^{(\alpha)} \quad z_3^{(\alpha)}]^T, z = [z_1 \quad z_2 \quad z_3]^T, \widehat{B} = [0 \quad \widehat{b} \quad 0], \text{ and}$$

$L = [\beta_1 \quad \beta_2 \quad \beta_3]^T$ are observer gains. z_1, z_2 and z_3 are the outputs of FESO: z_1 is the estimation of the state x_1 , z_2 is the estimation of the state x_2 , and z_3 is used to estimate the total disturbance x_3 . In addition, \widehat{b} is the estimated value of b , and $\widehat{b} \approx b$. To simplify the tuning process, the bandwidth-parameterization method [39] is employed. According to w -plane mapping (mentioned in Section 4), the FOS is translated into an integer order system in w -plane. By placing the poles of the translated characteristic equation $\lambda(w)$ in one location, the following is obtained

$$\lambda(w) = w^3 + \beta_1 w^2 + \beta_2 w + \beta_3 = (w + \omega_o)^3 \quad (11)$$

where, the observer gains can be linearized as

$$\begin{cases} \beta_1 = 3\omega_o \\ \beta_2 = 3\omega_o^2, \\ \beta_3 = \omega_o^3 \end{cases} \quad (12)$$

For the integer order system, variable ω_o is referred to as the bandwidth of ESO. When it comes to FOS, ω_o possesses the bandwidth characteristics. In order to facilitate distinction, the variable ω_o in (11) is considered to be the w -plane bandwidth of FESO. The main objective of FESO is to estimate the total disturbance in real time, and wider w -plane bandwidth will result in faster response. In practice, however, upper limitation of the bandwidth is related with the sampling ratio, and exceeding the limit will magnify sensor noises and dynamic uncertainties. A well-tuned ω_o must therefore make a balance between rapidity and stability [26,39,40]. The following Eq. (13) is used to test the FESO single parameter ω_o . Both of the two poles $-0.3125 \pm 1.0735i$ stay in the stable region (refer to Section 4 for details), that means the system of Eq. (13) is open-loop stable. Parameters $\omega_c = 20$, $\widehat{b} = b = 1.25$ and ω_o is set as $\{5, 50, 500, 1000\}$. The tracking responses are shown in Fig. 3

$$\frac{Y(s)}{U(s)} = \frac{1.25}{s^{1.8} + 0.625s^{0.9} + 1.25} \quad (13)$$

Fig. 3 shows that estimating ability of FESO is strengthened with the increase of the observer w -plane bandwidth. However, outputs of FESO become unstable when the w -plane bandwidth is beyond the toplimit. The upper limit is related to the sampling rate, and a higher sampling rate leads to a higher upper limit.

3.2. Design of fractional PD controller

Referring to Fig. 3, a well-tuned observer can track the extended state $f(y, y^{(\alpha)}, \omega)$ accurately. The control law can be designed as

$$u = \frac{-z_3 + u_0}{\widehat{b}}, \quad (14)$$

to obtain a desired response, where u_0 is a common linear fractional PD control:

$$u_0 = k_p(v_0 - z_1) + k_d(v_0^{(\alpha)} - z_2), \quad (15)$$

where k_p and k_d are controller gains. The parameters tuning is further simplified using the method in [39]

$$\begin{cases} k_d = 2\omega_c \\ k_p = \omega_c^2 \end{cases} \quad (16)$$

where ω_c is the w -plane bandwidth of the controller. Time derivative of the setpoint is omitted to avoid the pulse in [39]. However, because the fractional order differentiation of the step signal is a gradual process rather than the pulse signal, $v_0^{(\alpha)}$ cannot be omitted in (15). Then Eq. (7) becomes a commensurate cascade fractional order integrator form as

$$y^{(2\alpha)} \approx u_0. \quad (17)$$

Considering Eqs. (15) and (17), the following closed-loop transfer function can be obtained, namely, the desired response of FADRC is

$$\frac{Y(s)}{R(s)} \approx \frac{k_d s^\alpha + k_p}{s^{2\alpha} + k_d s^\alpha + k_p}. \quad (18)$$

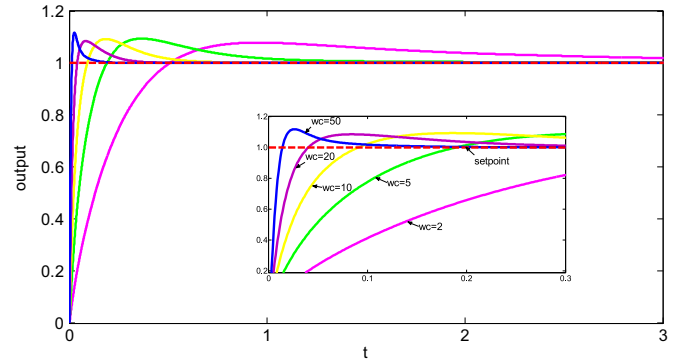


Fig. 5. System outputs with different ω_c .

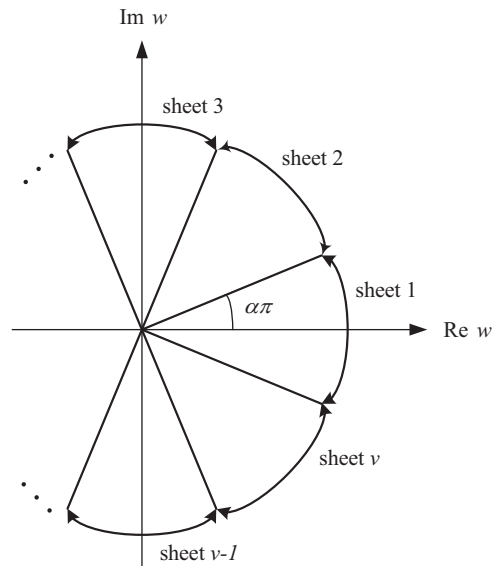


Fig. 6. The correspondence between the w -plane and s Riemann sheets.

Eq. (13) is taken as an example again, with fixed parameter $\widehat{b} = 1.25$. Fig. 4 shows the desired response and the output results with different ω_o ($\omega_c = 20$ is fixed). Fig. 5 shows the output responses with different controller w -plane bandwidth ω_c ($\omega_o = 200$ is fixed).

As Fig. 4 shows, the output results tracks closely to the desired response with the increase of ω_o . This is because the larger observer w -plane bandwidth can ensure precise disturbance estimation and then compensator can be applied to reject the total disturbance. Fig. 5 shows that small ω_c makes the system response slower, while large ω_c makes it faster.

In a practical application, the design procedure consists of two stages. In the first stage, a linear FESO is designed and a well-tuned ω_o is selected to ensure accurate estimations. In the second stage, a fractional order PD controller is designed under the assumption that the total disturbance is well estimated, and all the existing methods could be used in this stage for designing linear or non-linear controllers.

4. Root locus and frequency domain analysis for fractional active disturbance rejection control

A FOS can be generally expressed in the following form:

$$H(s) = \frac{b_m s^m + \dots + b_1 s^{\frac{1}{\nu}} + b_0}{a_n s^n + \dots + a_1 s^{\frac{1}{\nu}} + a_0} \quad (19)$$

where $a_k (k = 0, \dots, n), b_k (k = 0, \dots, m)$ are constants, and $\nu > 1$. The Riemann sheets are determined by using

$$s = |s|e^{j\phi}. \quad (20)$$

$$\Phi_r(s) = \frac{k_d s^{4\alpha} + (k_p + k_d \beta_1) s^{3\alpha} + (k_p \beta_1 + k_d \beta_2) s^{2\alpha} + (k_d \beta_3 + k_p \beta_2) s^\alpha + k_p \beta_3}{\frac{b}{G_p} [s^{3\alpha} + (\beta_1 + k_d) s^{2\alpha} + (\beta_1 k_d + \beta_2 + k_p) s^\alpha] + (k_p \beta_1 + k_d \beta_2 + \beta_3) s^{2\alpha} + (k_p \beta_2 + k_d \beta_3) s^\alpha + k_p \beta_3} \quad (24)$$

where $(2k+1)\pi < \theta < (2k+3)\pi$, and $k = -1, 0, \dots, \nu-2$. The Riemann sheet is named as the Principal Riemann Sheet when $k = -1$. Note that only roots lying on the Principal Riemann Sheet can determine the time-domain behavior and stability performance. These sheets are mapped to the w -plane as defined by

$$w = |w|e^{j\theta} \quad (21)$$

where $w = s^\alpha$ and $\alpha = 1/\nu$. The sheets can be projected to the w -plane by

$$\alpha(2k+1)\pi < \theta < \alpha(2k+3)\pi \quad (22)$$

The correspondence between the w -plane and s Riemann sheets is shown in Fig. 6. With the transformation of the w -plane, the stability of FOS can be predicted by the trend of root locus. The region of instability ($-\alpha\pi/2 \leq \arg(w) \leq \alpha\pi/2$) in the w plane corresponds to the right half plane ($-\pi/2 \leq \arg(s) \leq \pi/2$) in the s plane. The root locus branches never enter the unstable region,

which implies the system remains stable. Otherwise, if the root locus branches never enter the stable region, the system remains unstable. If the branches move from the stable region to the unstable region (or move from the unstable region to the stable region), then the range of grain can be determined [30,31,41,42].

4.1. Root locus of linear fractional order systems

The steps to plot the root loci of FOS are listed as follow:

- a) Attain the open loop transfer function of FOS;
- b) Transform FOS into an integer order system on the w -plane;
- c) Obtain the root locus of the transformed system;
- d) Identify the Principal Riemann Sheets and the unstable region on the w -plane;
- e) Perform stability analysis from the root locus on the w -plane.

In order to analyze the stability of FADRC, the FADRC time domain configuration shown in Fig. 2 is changed into a frequency domain block diagram form [42]. As Fig. 7 shows, $V_o(s)$ and $Y(s)$ represent the setpoint and output, respectively; Ω denotes the external disturbance; $G_p(s)$ is the transfer function of a commensurate linear FOS.

The other transfer functions in the blocks are listed in Appendix A. By the equivalent transformation of the block diagram, the close-loop transfer function can be obtained as follows when the effect of the external disturbance Ω is omitted.

$$\Phi_r(s) = \frac{Y(s)}{V_o(s)} = \frac{G_{r1} G_c G_p + G_{r2} G_p}{b + G_p G_{f1} + G_c G_p G_{f2}} \quad (23)$$

and

Taking Eq. (7) as an example, the parameters of FADRC are designed using Eqs. (12) and (16). Then, the open loop transfer function of $\Phi_r(s)$ can be written as

$$\Phi_o(s) = \frac{\Phi_r(s)}{1 - \Phi_r(s)} \quad (25)$$

and

$$\Phi_o(s) = \frac{k_d s^{4\alpha} + (k_p + k_d \beta_1) s^{3\alpha} + (k_p \beta_1 + k_d \beta_2) s^{2\alpha} + (k_d \beta_3 + k_p \beta_2) s^\alpha + k_p \beta_3}{\frac{b}{G_p} [s^{3\alpha} + (\beta_1 + k_d) s^{2\alpha} + (\beta_1 k_d + \beta_2 + k_p) s^\alpha] - k_d s^{4\alpha} - (k_p + k_d \beta_1) s^{3\alpha} + \beta_3 s^{2\alpha}} \quad (26)$$

For different kinds of objects, two categories are studied to discuss their root loci:

4.1.1. For the commensurate fractional order system

When $G_p(s) = \frac{b}{s^{2\alpha} + a_2 s^\alpha + a_1}$ and $\frac{b}{b} \approx 1$, the open loop transfer function can be written as

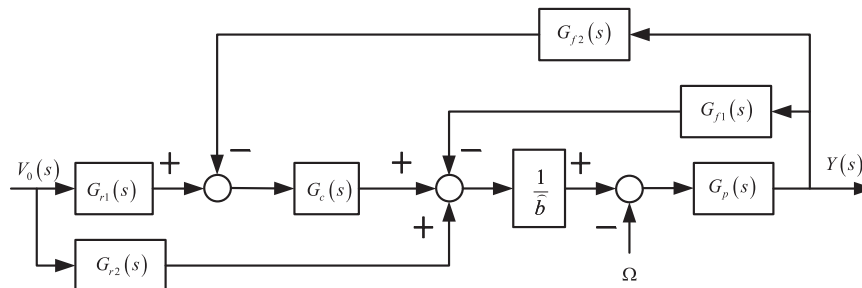


Fig. 7. Block diagram of the FADRC in frequency domain.

$$\Phi_o(s) = \frac{k_d s^{4\alpha} + (k_p + k_d \beta_1) s^{3\alpha} + (k_p \beta_1 + k_d \beta_2) s^{2\alpha} + (k_d \beta_3 + k_p \beta_2) s^\alpha + k_p \beta_3}{s^{5\alpha} + (\beta_1 + a_2) s^{4\alpha} + (\beta_2 + \beta_1 a_2 + k_d a_2 + a_1) s^{3\alpha} + (\beta_1 k_d a_2 + \beta_2 a_2 + k_p a_2 + \beta_1 a_1 + k_d a_1 + \beta_3) s^{2\alpha} + (\beta_1 k_d a_1 + \beta_2 a_1 + k_p a_1) s^\alpha} \quad (27)$$

Fig. 8 shows the root locus when $\alpha=0.9$, $a_1=1.25$, $a_2=0.625$, $\widehat{b}=b=1.25$, $\omega_o=100$ and $\omega_c=20$, the open loop poles and zeros are given in Table 1.

4.1.2. For the incommensurate fractional order system

When $G_p(s) = \frac{b}{s^{2\alpha} + a_2 s^{\alpha+\delta} + a_1}$ and $\widehat{b} \approx 1$, the open loop transfer function can be written as

$$\Phi_o(s) = \frac{k_d s^{4\alpha} + (k_p + k_d \beta_1) s^{3\alpha} + (k_p \beta_1 + k_d \beta_2) s^{2\alpha} + (k_d \beta_3 + k_p \beta_2) s^\alpha + k_p \beta_3}{\widehat{b} [s^{2\alpha} + a_2 s^{\alpha+\delta} + a_1] [s^{3\alpha} + (\beta_1 + k_d) s^{2\alpha} + (\beta_1 k_d + \beta_2 + k_p) s^\alpha] - k_d s^{4\alpha} - (k_p + k_d \beta_1) s^{3\alpha} + \beta_3 s^{2\alpha}} \quad (28)$$

Fig. 9 shows the root locus when $\alpha=0.9$, $\delta=-0.3$, $a_1=1.25$, $a_2=0.625$, $\widehat{b}=b=1.25$, $\omega_o=100$ and $\omega_c=20$, the open loop poles and zeros are given in Table 1. Fig. 10 shows the root locus when $\alpha=0.9$, $\delta=0.3$, $a_1=1.25$, $a_2=0.625$, $\widehat{b}=b=1.25$, $\omega_o=100$

and $\omega_c=20$, and the open loop poles and zeros are given in Table 1.

From the root loci in Figs. 8–10, it is clear that all the curves are in the stable region and have no intersections with the stability boundary. In other words, the system remains stable for all gain values. Although the objects are not the standard commensurate FOS ($\delta \neq 0$), the proposed method is also applicable.

4.2. Frequency-domain characteristics analysis

Frequency domain characteristics are widely used to analyze automatic control systems in classical control theory. Bode

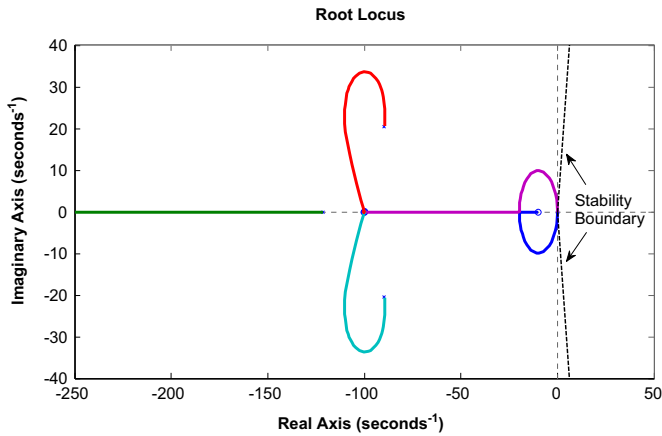


Fig. 8. Root locus when $\alpha=0.9$, $a_1=1.25$, $a_2=0.625$, $\widehat{b}=b=1.25$, $\omega_o=100$ and $\omega_c=20$, where the dotted line is the stability boundary.

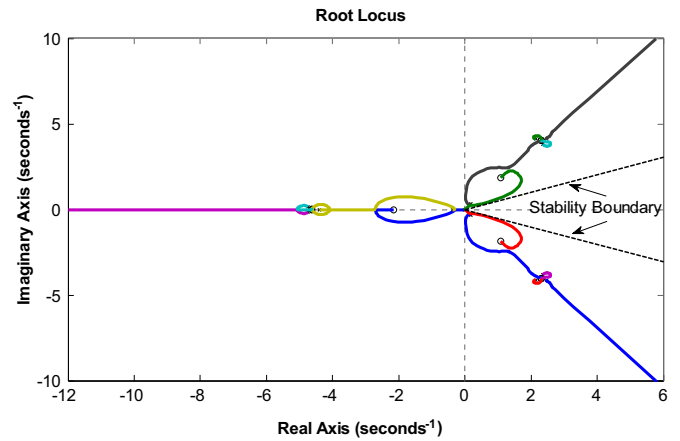


Fig. 9. Root locus when $\alpha=0.9$, $\delta=-0.3$, $a_1=1.25$, $a_2=0.625$, $\widehat{b}=b=1.25$, $\omega_o=100$ and $\omega_c=20$, where the dotted line is the stability boundary.

Table 1
Open loop zeros and poles for different objects.

Objects		Instability region	Zeros	Poles
$\alpha=0.9$ $a_1=1.25$ $a_2=0.625$	$\delta=0$ (Fig. 8)	$-\frac{9}{20}\pi \leq \arg(w) \leq \frac{9}{20}\pi$	$w_{1,2,3} = -100$ $w_4 = -10$	$w_1 = 0$ $w_2 = -121.4$ $w_{3,4} = -89.6 \pm 20.5i$ $w_5 = -0.05$
$b=1.25$ $\widehat{b}=1.25$	$\delta=-0.3$ (Fig. 9)	$-\frac{3}{20}\pi \leq \arg(w) \leq \frac{3}{20}\pi$	$w_{1,2,3} = -4.64$ $w_{4,5,6} = 2.32 + 4.02i$ $w_{7,8,9} = 2.32 - 4.02i$ $w_{10} = -2.15$ $w_{11,12} = 1.08 \pm 1.87i$	$w_{1,2,3} = 0$ $w_{4,5} = -4.76 \pm 0.17i$ $w_6 = -4.40$ $w_{7,8} = 2.47 \pm 4.14i$ $w_{9,10} = 2.14 \pm 4.11i$ $w_{11,12} = 2.37 \pm 3.80i$ $w_{13} = -0.38$ $w_{14,15} = 0.18 \pm 0.33i$
$\omega_o=100$ $\omega_c=20$	$\delta=0.3$ (Fig. 10)	$-\frac{3}{20}\pi \leq \arg(w) \leq \frac{3}{20}\pi$	$w_{1,2,3} = -4.64$ $w_{4,5,6} = 2.32 + 4.02i$ $w_{7,8,9} = 2.32 - 4.02i$ $w_{10} = -2.15$ $w_{11,12} = 1.08 \pm 1.87i$	$w_{1,2,3} = 0$ $w_{4,5} = 2.43 \pm 4.51i$ $w_{6,7} = 2.83 \pm 3.73i$ $w_{8,9} = 1.66 \pm 3.88i$ $w_{10,11} = -4.96 \pm 0.42i$ $w_{12} = -3.92$ $w_{13} = -0.38$ $w_{14,15} = 0.19 \pm 0.32i$

diagram is an important component for the frequency-domain analysis. The closed-loop stability, rapidity and accuracy can be analyzed based on the bode diagram. A basic feedback frame can be obtained from the frequency-domain block diagram of Fig. 7, and the equivalent open-loop transfer function is described in Eq.

(26). Taking Eq. (13) as an example, the Bode diagram with different ω_c ($\omega_o=200$ is fixed), is shown in Fig. 11(a) and the bode diagram with different ω_o ($\omega_c=50$ is fixed) is shown in Fig. 11(b).

Fig. 11(a) shows that the crossover frequency becomes bigger with the increase of ω_c . This means that a bigger ω_c makes the system response more quickly. In addition, the phase margin keeps almost unchanged, which ensures the stability of the system. It can be seen from Fig. 11(b) that the system almost has almost the same bode diagram in the low frequency interval for different ω_o , which means the observer w -plane bandwidth ω_o has little effect on the stability.

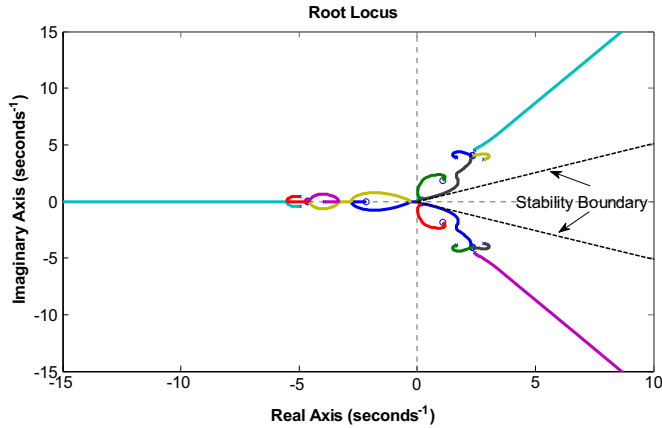
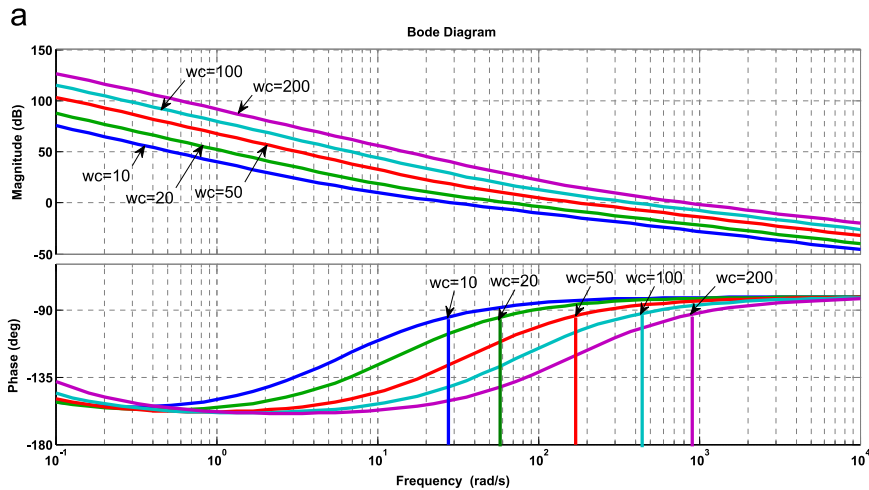


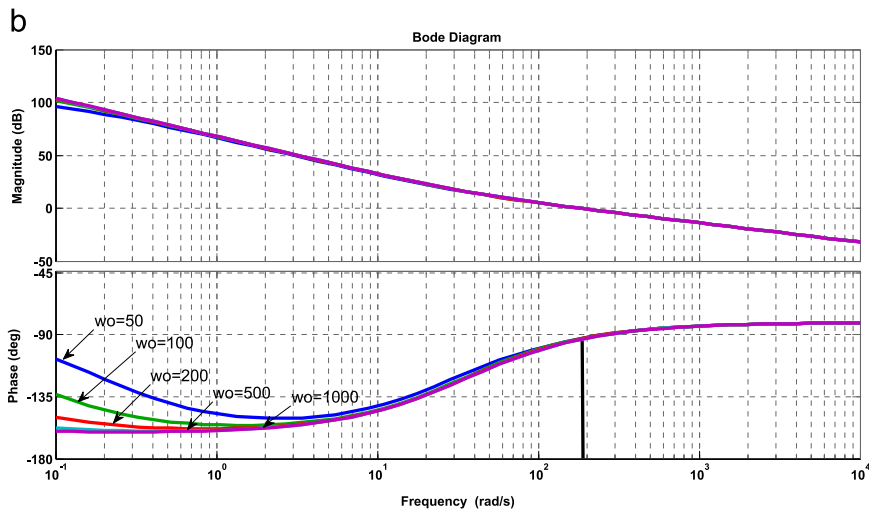
Fig. 10. Root locus when $\alpha=0.9$, $\delta=0.3$, $a_1=1.25$, $a_2=0.625$, $b=1.25$, $\omega_o=100$ and $\omega_c=20$. The dotted line is the stability boundary.

5. Simulation and discussion

In this section, simulation results for four different FOS are implemented to verify the superiority and effectiveness of the proposed method. The methods in [43] and [26] are adopted to design ADRC for FOS control (see Table 2). In Table 2, comparative results with method in [43] are listed in No. 1 and comparative results with method in [26] are listed in No. 2–5. For the sake of fairness, the transition process of the setpoint generated by TD is added in FADRC and ADRC, and the second order TD can be designed as [21]



Bode diagram with different ω_c ($\omega_o=200$ is fixed).



Bode diagram with different ω_o ($\omega_c=50$ is fixed).

Fig. 11. Bode diagrams with different parameters. (a) Bode diagram with different ω_c ($\omega_o=200$ is fixed). (b) Bode diagram with different ω_o ($\omega_c=50$ is fixed).

Table 2
Controller parameters and performance indices.

No.	Objects	Parameters $\{\omega_o, \omega_c, \widehat{b}, T\}$		ISE (10^{-5})	
		FADRC	Comparative method	FADRC	Comparative method
1.	Commensurate nonlinear FOS	$\{30, 5, 1, 0.001\}$	$\omega_o=30, k_p=10, k_i=2, k_d=1, \lambda=0.8, \widehat{b}=1, T=0.001$	3000	45,000
2.	Gas-turbine model (at 90% rated speed)	$\{100, 10, 14165, 0.001\}$		670	1000
3.	Gas-turbine model (at 93% rated speed)	$\{100, 10, 8533, 0.001\}$		340	660
4.	Heat-solid model	$\{300, 10, 0.0252, 0.0001\}$		35.3	37.5
		$\{30, 10, 0.0252, 0.0001\}$		35.3	120
5.	Solid-core active magnetic bearing	$\{4000, 200, 5600, 0.0001\}$		1.2	68

$$\begin{cases} \dot{v}_1 = v_2 \\ \dot{v}_2 = fhan(v_1 - v_0, v_2, r, h) \end{cases} \quad (29)$$

where v_0 is the setpoint, v_1 is the transition process of v_0 , v_2 is the differential trajectory of v_1 , r and h are adjustable parameters, and the function $fhan(\cdot)$ is defined as:

$$fhan(x_1, x_2, r, h) = - \begin{cases} r \text{sign}(a), |a| > d \\ r \frac{a}{d}, |a| \leq d \end{cases}, \quad (30)$$

where a and d are given as follows:

$$\begin{cases} d = rh; \\ d_0 = hd; \\ y = x_1 + hx_2; \\ a_0 = \sqrt{d^2 + 8r|y|}; \\ a = \begin{cases} x_2 + \frac{(a_0 - d)\text{sign}(y)}{2}, |y| > d_0 \\ x_2 + \frac{y}{h}, |y| \leq d_0 \end{cases} \end{cases} \quad (31)$$

All the parameters and assessment indices are listed in Table 2, where T is the sampling time; ISE is the short for integral square error: $ISE(t) = \int_0^t (y(t) - v_1(t))^2 dt$.

5.1. A commensurate nonlinear fractional order system

The following commensurate nonlinear FOS is used to compare the performance between FADRC and the Gao's method [43].

$$\begin{cases} D^{0.8}x_1(t) = x_2(t) \\ D^{0.8}x_2(t) = \sin(x_2(t)) + x_2(t) + u(t). \\ y(t) = x_1(t) \end{cases} \quad (32)$$

The reference input is $v(t)=5$, and the parameters of FADRC and Gao's method are listed in Table 2. Fig. 12(a) shows the transition process and closed loop output of Eq. (32), and Fig. 12(b) shows the control signals.

As Fig. 12 shows, FADRC can track the transition process with less oscillation, and FADRC's control signal is also reasonable. It can be seen that the commensurate nonlinear FOS is well controlled by FADRC. In addition, the total variation(TV) of the control effort is used to compare the performance of different controllers. The definition of TV index is given as follows:

$$TV = \sum_{i=1}^{\infty} |u_{i+1} - u_i|. \quad (33)$$

TV obtained for FADRC is 26.1 and that for Gao's method is 44.1, which shows that FADRC owns smaller control effort. This is beneficial for practical application.

5.2. Gas turbine plant

The model of the fractional order gas turbine plant, which converts the fuel energy into an useful form, is given by Nataraj

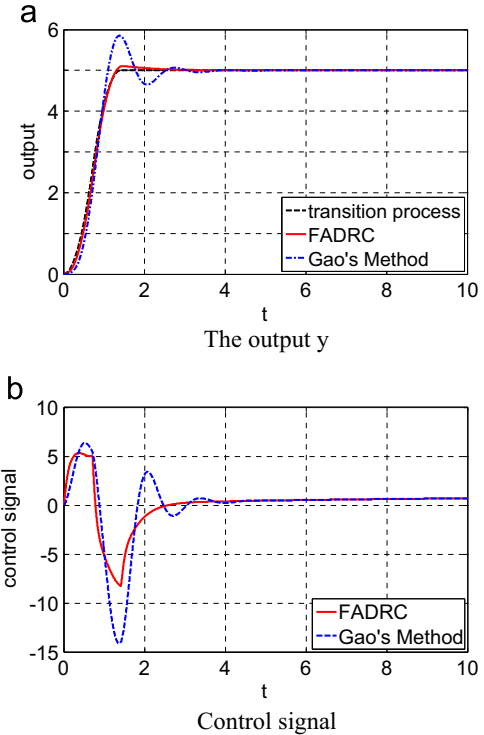


Fig. 12. Outputs comparison between FADRC and Gao's method. (a) The output y . (b) Control signal.

[44]. The input and output of the gas turbine are fuel rate and turbine speed, respectively. For the operating regime at 90% rated speed, the fractional order model is

$$G_{90\%}(s) = \frac{103.9705}{0.00734s^{1.6807} + 0.1356s^{0.8421} + 1}. \quad (34)$$

For another operating regime at 93% rated speed, the fractional order model is

$$G_{93\%}(s) = \frac{110.9238}{0.0130s^{1.6062} + 0.1818s^{0.7089} + 1}. \quad (35)$$

Fig. 13 shows the output responses for the operating regime at 90% and 93% of rated speed demand. The well-tuned parameters of FADRC and ADRC are listed in Table 2.

Fig. 13(a) and (c) shows FADRC has faster adjustment capability. Fig. 13(b) and (d) shows the corresponding control signals.

5.3. Heat-solid model

A heat solid model is described by the following fractional order transfer function [45]

$$G(s) = \frac{1}{39.69s^{1.26} + 0.598}. \quad (36)$$

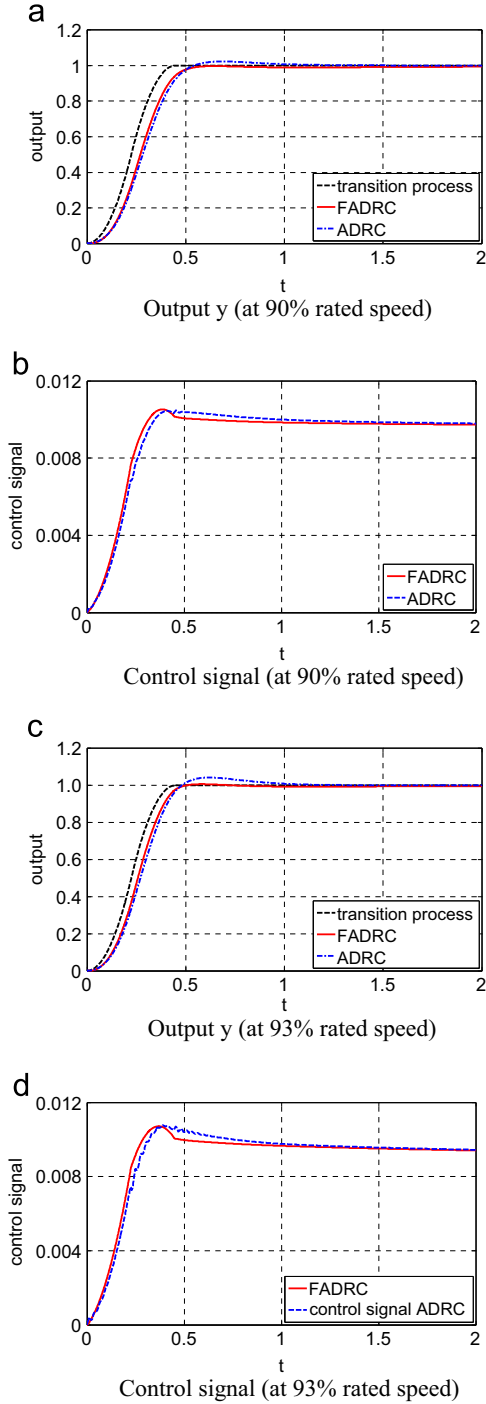


Fig. 13. Response comparisons between FADRC and ADRC on gas-turbine model. (a) Output y (at 90% rated speed). (b) Control signal (at 90% rated speed). (c) Output y (at 93% rated speed). (d) Control signal (at 93% rated speed).

The input and output are voltages, and least squares method is used to identify the unknown parameters. A FADRC is designed with the commensurate order $\alpha=0.63$, and the total disturbances is $f_{FADRC} = -0.598/39.69y$. A first-order ADRC/second-order ESO is used for comparison. The total disturbance is $f_{ADRC} = y^{(1)} - y^{(1.26)} - 0.598/39.69y$. Parameters of FADRC and ADRC are listed in Table 2. Simulation results with $\omega_o=300$ and $\omega_o=30$ are shown in Fig. 14(a) and (b), respectively.

It can be seen from Fig. 14 and Table 2 that FADRC has a better response. It is also important to note that FADRC is able to respond quickly even with a relatively small bandwidth (see Fig. 14(b)), which makes the solution more practical.

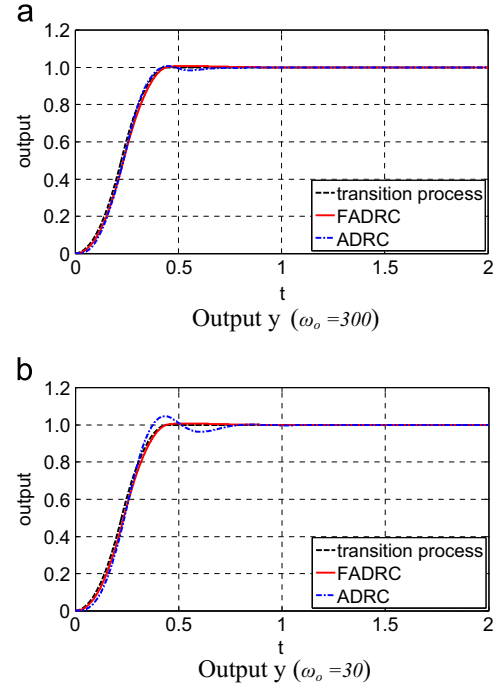


Fig. 14. Response comparison between FADRC and ADRC on heat-solid model. (a) Output y ($\omega_o=300$). (b) Output y ($\omega_o=30$).

5.4. Solid-core active magnetic bearing

Due to the eddy current effect, a solid-core active magnetic bearing (AMB) shows some fractional order characteristics and the traditional magnetic equivalent circuit model has significant amounts of errors when predicting the actual system. A weighted least-squares method was derived for the general fractional model based on the widely studied commensurate order fractional model in [46]. The final results show that the identified fractional model structure is closer to the actual system, and the result is:

$$G(s) = \frac{5594.32}{s^{2.75} + 259.08s^{1.83} - 85950.3s^{0.79} - 14240336.8} \quad (37)$$

Typically, the AMB model is close to the third order linear FOS with the commensurate order $\alpha=0.9$, and a third order FADRC is therefore adopted for the control of the plant. Parameters of FADRC and ADRC are listed in Table 2.

Fig. 15 shows that third-order FADRC has faster adjustment capability. Furthermore, FESO can get precise estimations when the observer w -plane bandwidth is increased to 1000. For ESO, however, the precise estimations are not available until the observer bandwidth is increased to 4000. This means that FADRC does not require higher bandwidth or sampling rate and is more suitable for practical engineering.

5.5. Robust analysis

A robustness assessment is carried out about the parameters of Eq. (13). The following plant (38) with uncertain parameters δ and ε are considered:

$$y^{(1.8+\varepsilon)} = \left(-\frac{5}{8}y^{(0.9+\delta)} - \frac{10}{8}y \right) + \frac{10}{8}u. \quad (38)$$

The normalized integral square error (ISE) trajectory tracking performance indices are used as

$$\begin{cases} ISE_v(t) = \int_0^t (y(t) - v_1(t))^2 dt \\ ISE_f(t) = \int_0^t (f(t) - z_3(t))^2 dt \end{cases} \quad (39)$$

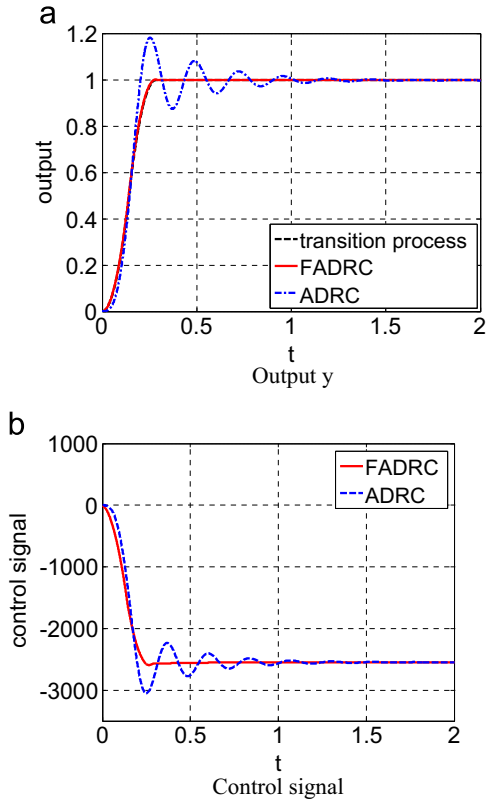


Fig. 15. Response comparison between FADRC and ADRC on solid-core active magnetic bearing. (a) Output y . (b) Control signal.

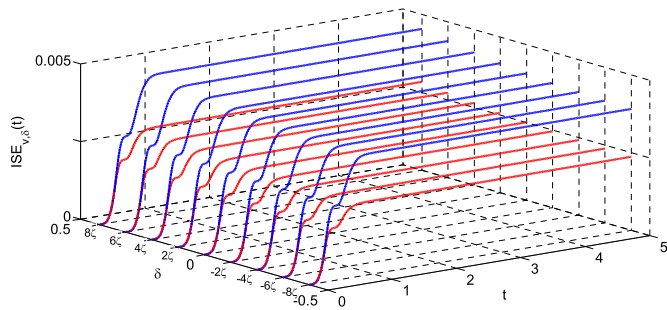


Fig. 16. Behavior of the output ISE trajectories for different values of the uncertainty order δ , when $\varepsilon=0$ is fixed (Red full line indicates FADRC, blue dotted line indicates ADRC and the step is 2ζ . For interpretation of the references to color in this figure legend, the reader is referred to the web version of this article.)

where $v_1(t)$ is the transition process of the setpoint and $f(t)$ is the total disturbance. Considering the dynamic characteristic of the system and the accuracy of the identification method, the variation of uncertain parameter ε is set between -0.25 and 0.25 . As the second item produces small effects on the system, and parameter δ is set between -0.5 and 0.5 . Figs. 16 and 17 show the trajectories of $ISE_{v,\delta}(t)$ and $ISE_{f,\delta}(t)$ for different uncertain parameters of δ in step of 2ζ , when $\varepsilon=0$ is fixed and $\zeta = (\sqrt{3} - \sqrt{2})/6$. Fig. 17 and Fig. 18 show the trajectories $ISE_{v,\varepsilon}(t)$ and $ISE_{f,\varepsilon}(t)$ for different uncertain parameters of ε in step of ζ , when $\delta=0$ is fixed.

From Fig. 16 to Fig. 19, the following conclusions can be obtained. 1). For different uncertain parameters δ , Figs. 16 and 17 show that FADRC owns smaller ISE value in both the output and disturbance trajectories. This means that FADRC could track trajectory (setpoint or total disturbance) more quickly and precisely. The constant steady states of these loci indicate that the corresponding outputs are ultimately close to the desired reference trajectories. 2). When the uncertain parameter ε changes, the

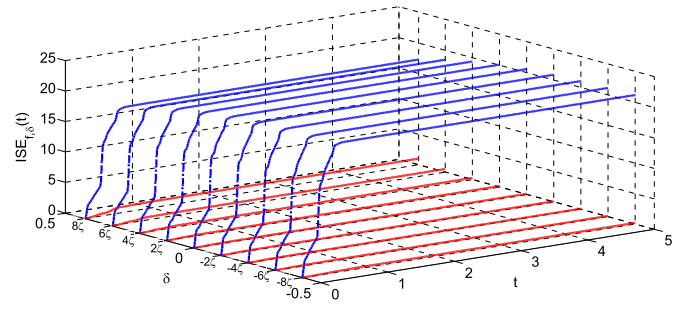


Fig. 17. Behavior of the disturbance ISE trajectories for different values of uncertainty order δ , when $\varepsilon=0$ is fixed (Red full line indicates FADRC, blue dotted line indicates ADRC and the step is 2ζ . For interpretation of the references to color in this figure legend, the reader is referred to the web version of this article.)

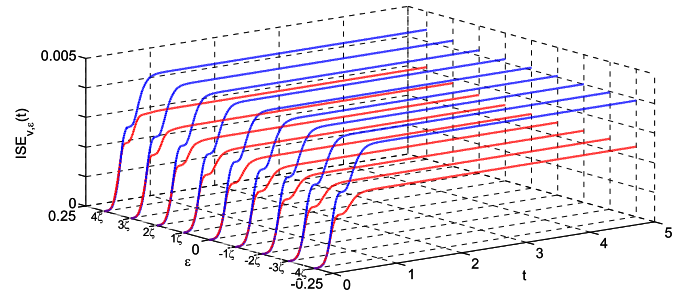


Fig. 18. Behavior of the output ISE trajectories for different values of the uncertainty order ε , when $\delta=0$ is fixed (Red full line indicates FADRC, blue dotted line indicates ADRC and the step is ζ . For interpretation of the references to color in this figure legend, the reader is referred to the web version of this article.)

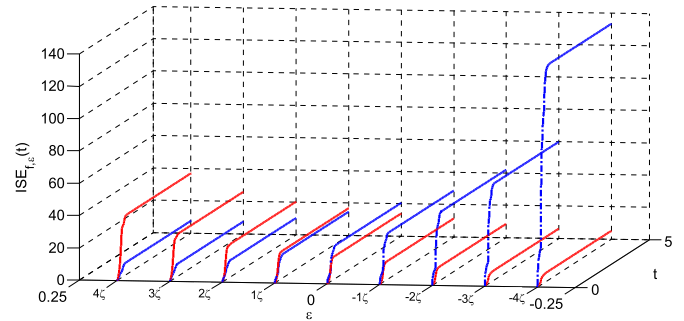


Fig. 19. Behavior of the disturbance ISE trajectories for different values of uncertainty order ε , when $\delta=0$ is fixed (Red full line indicates FADRC, blue dotted line indicates ADRC and the step is ζ . For interpretation of the references to color in this figure legend, the reader is referred to the web version of this article.)

advantages of FADRC are distinct. Figs. 18 and 19 show that FADRC obtains better performance when the first item $1.8 + \varepsilon$ is changed, while FESO is affected by the modification of ε . When $1.8 + \varepsilon$ is closer to 2, the ESO achieve a better performance. This is a good example to prove that FADRC is necessary for a system with an integer-distancing fractional order. 3). The highest order of FOS plays an important role in FADRC designing for different system because the no-highest items are treated as the total disturbance and rejected by the controller. 4). More importantly, FADRC could track the trajectory quickly and precisely even if there exist a large change of uncertain parameter δ and ε , which means the FADRC is also appropriate for incommensurate linear FOS.

6. Conclusion

The traditional ADRC solution for FOS is improved in this paper, where the ESO and the NLSEF are replaced by FESO and PD^α

controller respectively. Linear bandwidth-parameterization method is applied to simplify the parameters tuning. In addition, stability and frequency-domain characteristics of FADRC for FOS are also analyzed. Numerical simulations show the superiority and effectiveness of the proposed scheme over the existing ADRC solution. Moreover, robustness analysis shows that FADRC is also appropriate for incommensurate FOS control. Furthermore, it is believed that further improvements can be obtained by employing the nonlinear gains in FADRC but it would require a thorough theoretical study of necessity.

Acknowledgments

This research has been supported by the National Natural Science Foundation of P.R. China (Grant No. 61573052).

Appendix: A

The transfer functions of the blocks in Fig. 7 are

$$G_{r1}(s) = \frac{k_d s^\alpha + k_p}{s^{2\alpha} + (\beta_1 + k_d) s^\alpha + (\beta_1 k_d + \beta_2 + k_p)} \quad A-1$$

$$G_{r2}(s) = \frac{k_d s^{3\alpha} + (k_p + k_d \beta_1) s^{2\alpha} + (k_p \beta_1 + k_d \beta_2) s^\alpha + k_p \beta_2}{s^{2\alpha} + (\beta_1 + k_d) s^\alpha + (\beta_1 k_d + \beta_2 + k_p)} \quad A-2$$

$$G_{f1}(s) = \frac{(k_p \beta_1 + k_d \beta_2) s^\alpha + k_p \beta_2}{s^{2\alpha} + (\beta_1 + k_d) s^\alpha + (\beta_1 k_d + \beta_2 + k_p)} \quad A-3$$

$$G_{f2}(s) = \frac{s^{2\alpha} + k_d s^\alpha + k_p}{s^{2\alpha} + (\beta_1 + k_d) s^\alpha + (\beta_1 k_d + \beta_2 + k_p)} \quad A-4$$

$$G_c = \frac{\beta_3}{s^\alpha} \quad A-5$$

References

- [1] Skaar SB, Michel AN, Miller RK. Stability of viscoelastic control system. *IEEE Trans Autom Control* 1988;33(4):348–57.
- [2] Chen Y, Moore KL. Analytical stability bound for a class of delayed fractional-order dynamic systems. In: Proceedings of the 40th IEEE conference on decision and control; 2001. p. 1421–6.
- [3] Mandelbrot B, Member S. Some noise with 1/f spectrum, a bridge between direct current and white noise. *IEEE Trans Inform Theory* 1967;2(13):289–98.
- [4] Tsai JS, Chien T, Guo S, Chang Y, Shieh L. State-space self-tuning control for stochastic fractional-order chaotic systems. *IEEE Trans Circuits Syst I. Regular paper*. 54(3); 2007. p. 632–42.
- [5] Reyes-Melo ME, Martinez-Vega JJ, Guerrero-Salazar CA, Ortiz-Mendez U. Application of fractional calculus to modelling of relaxation phenomena of organic dielectric materials. In: Proceedings of the 2004 International conference on solid dielectrics; 2004. p. 530–3.
- [6] Friedrich C. Relaxation and retardation functions of the Maxwell model with fractional derivatives. *Rheol Acta* 1991;30(2):151–8.
- [7] Liu D, Laleg-Kirati T, Gibaru O, Perruquetti W. Identification of fractional order systems using modulating functions method. In: Proceedings of the 2013 American control conference (ACC); 2013. p. 1679–85.
- [8] Idiou D, Charef A, Djouambi A. Linear fractional order system identification using adjustable fractional order differentiator. *IET Signal Process* 2013;4(8):398–409.
- [9] Li D, Fan W, Gao Y, Jin Q. Iterative least square identification algorithm for fractional order system. *J Jiangnan Univ: Nat Sci Ed* 2010;9(4):404–8.
- [10] Charef A, Idiou D, Djouambi A, Voda A. Identification of linear fractional systems of commensurate order. In: Proceedings of the 3rd international conference on systems and control; 2013. p. 259–64.
- [11] Chen Y. Ubiquitous fractional order controls. In: Proceedings of the Second IFAC symposium on fractional derivatives applications; 2006. p. 481–92.
- [12] Chen Y, Petras I, Xue D. Fractional order control-A tutorial. In: Proceedings of the 2009 American control conference; 2009. p. 1397–411.
- [13] Oustalout A, Bansard M. First generation CRONE control. In: Proceedings of conference on system, man and cybernetic, 1993' systems engineering in the service of humans'; 1993. p. 130–5.
- [14] Oustalout A, Bluteau B, Lanusse P. Second generation CRONE control. In: Proceedings of conference on system, man and cybernetic, 1993' systems engineering in the service of humans'; 1993. p. 136–42.
- [15] Oustalout A, Melchior P, Lanusse P, Cois O, Dancla F. The CRONE toolbox for Matlab. CACSD. In: Proceedings of Conference on IEEE International symposium on computer-aided control system design; 2000. p. 190–5.
- [16] Lurie BJ. Three-parameter tunable tilt-integral-derivative (TID) controller. Patent, US; 1994.
- [17] Podlubny I. Fractional-order systems and pid controllers. *IEEE Trans Autom Control* 1999;1(44):208–14.
- [18] Li D, Liu L, Jin Q, Hirasawa K. Maximum sensitivity based fractional IMC-PID controller design for non-integer order system with time delay. *J Process Control* 2015;31:17–29.
- [19] Raynaud HF, Zergainoh A. State-space representation for fractional order controllers. *Automatica* 2000;36(7):1017–21.
- [20] Han J. Auto-disturbances-rejection controller and its application. *Control Decis* 1998;13(01):19–23.
- [21] Han J. Active disturbance rejection control technique. Beijing: National Defense Industry Press; 2008.
- [22] Han J. From PID to active disturbance rejection control. *IEEE Trans Ind Electron* 2009;56(3):900–6.
- [23] Tian G, Gao Z. Benchmark tests of active disturbance rejection control on an industrial motion control platform. In: Proceedings of the 2009 conference on American control conference; 2009. p. 5552–7.
- [24] Sun L, Dong J, Li D, Lee KY. A practical multivariable control approach based on inverted decoupling and decentralized active disturbance rejection controller. *Ind Eng Chem Res* 2016. <http://dx.doi.org/10.1021/acs.iecr.5b03738>.
- [25] Xia Y, Dai L, Fu M, Li C, Wang C. Application of active disturbance rejection control in tank gun control system. *J Frankl Inst* 2014;351(4):2299–314.
- [26] Li M, Li D, Wang J, Zhao C. Active disturbance rejection control for fractional-order system. *ISA Trans* 2013;52(3):365.
- [27] Yang X, Huang Y. Capabilities of extended state observer for estimating uncertainties. In: Proceedings of the 2009 American control conference; 2009. p. 3700–5.
- [28] Tian G, Gao Z. Frequency response analysis of active disturbance rejection based control system. In: Proceedings of the 16th IEEE international conference on control applications part of IEEE multi-conference on systems and control; 2007. p. 1595–9.
- [29] Wu D, Ken C. Frequency-domain analysis of nonlinear active disturbance rejection control via the describing function method. *IEEE Trans Ind Electron* 2013;60(9):3906–14.
- [30] Tan N, Faruk Özgüven Ö, Mine Özyetkin M. Robust stability analysis of fractional order interval polynomials. *ISA Trans* 2009;48(2):166–72.
- [31] Patil MD, Vyawahare VA, Bhole MK. A new and simple method to construct root locus of general fractional-order systems. *ISA Trans* 2014;53(2):380–90.
- [32] Robert P. Noise-filtering properties of numerical methods for the inverse Abel transform. *IEEE Trans Instrum Meas* 1992;41(4):517–22.
- [33] Freeborn TJ, Maundy B, Elwakil A. Second order approximation of the fractional laplacian operator for equal-ripple response. In: Proceedings of the 53rd IEEE international midwest symposium on circuits and systems (MWSCAS); 2010. p. 1173–6.
- [34] Hartley TT, Lorenzo CF, Killory Qammer. H. Chaos in a fractional order Chua's system. *IEEE Trans Circuits Syst I: Fundam Theory Appl* 1995;42(8):485–90.
- [35] Podlubny I. Fractional differential equations. San Diego, CA: Academic Press; 1999.
- [36] Wang J, Xiao H. Design of fractional order state observer with full-dimensionality. *J Chongqing Univ Posts Telecommun: Nat Sci Ed* 2009;21(6):795–814.
- [37] Gao Z. Active disturbance rejection control: a paradigm shift in feedback control system design. In: Proceedings of the 2006 American control conference; 2006. p. 2399–405.
- [38] Ramírez-Neria M, Sira-Ramírez H, Garrido-Moctezuma R, Luviano-Juárez A. Linear active disturbance rejection control of underactuated systems: the case of the Furuta pendulum. *ISA Trans* 2014;53(4):920–8.
- [39] Gao Z. Scaling and bandwidth-parameterization based controller tuning. In: Proceedings of the 2003 American control conference; 2003. p. 4989–96.
- [40] Wang G, He Z. Control system design. Beijing: Tsinghua University Press; 2008.
- [41] Monje CA, Chen Y, Vinagre BM, Xue D, Feliu V. Fractional-order systems and controls. *Adv Ind Control* 2010.
- [42] Das S. Functional fractional calculus for system identification and controls. Berlin: Springer; 2008.
- [43] Gao Z. Active disturbance rejection control for nonlinear fractional-order systems. *Int J Robust Nonlinear Control* 2015.
- [44] Nataraj PSV, Kalla R. Computation of spectral sets for uncertain linear fractional-order systems. *Commun Nonlinear Sci Numer Simul* 2010;15:946–55.
- [45] Petráš I, Dorcák L, Košťál I. A comparison of the integer and the fractional order controllers on the laboratory object. In: Proceedings of ICAMC98/ASRTP'98; 1998. p. 451–4.
- [46] Zhong J, Li L. Fractional-order system identification of a solid-core active magnetic bearing. *Proc CSEE* 2013;33(18):170–7.